Energy Harvesting from Wind-induced Vibrations

Mohammed Ali, Mustafa Arafa, and Mohamed Elaraby

Abstract—The aim of this work is to exploit flow-induced vibration for energy harvesting. A cantilever beam carrying a tip mass in the form of a lightweight box having a square, triangular, or semicircular cross-section is designed to undergo galloping oscillations when subjected to an incoming wind stream. Electrical power is extracted from the self-excited flexural vibration of the beam through an electromagnetic generator consisting of a permanent magnet that is attached to the beam oscillating past a stationary coil. A theoretical model is developed to predict the system dynamics in terms of its design parameters. Emphasis is placed on developing finite element models to assess the lift and drag coefficients, together with their variation with the angle of attack, which are known to affect the aero-elastic behavior significantly. The resulting predictions of the lift and drag forces are then implemented in an electro-aeroelastic model to predict the output voltage and power. The results are supported by experimental measurements over a range of load resistance.

Index Terms—Energy Harvesting, Galloping, Wind-induced Vibrations.

1. INTRODUCTION

THE worldwide quest to exploit renewable energy sources has recently prompted significant research in the field of energy harvesting wherein clean useful energy is generated by novel means from existing ambient sources that are otherwise neglected. A number of ambient energy sources have been recognized to be promising for energy harvesting, including waste heat, mechanical vibration, wind, solar energy, rainfall, human movement, seismic forces, traffic, and sea waves. While most of these sources can be exploited for energy harvesting, mechanical vibration seems particularly appealing due to the convenience of directly converting mechanical energy into electrical energy through various well-established piezoelectric [1], electromagnetic [2] and electrostatic [3] transducers. A review of the pertinent literature reveals that most of the reported studies are based on the fact that mechanical vibration is readily available as a source of energy at our disposal. Emphasis in many studies was placed upon converting mechanical energy, typically provided by a dynamic shaker in a laboratory, into electrical energy. While these shaker tests provide useful tools to assess the performance of the developed devices at favorable drive conditions, further efforts are needed to expand the range of possibilities wherein mechanical vibration can be induced from clean and renewable sources for improved energy extraction in broader applications. An ideal candidate in this capacity is wind.

Wind power can be harvested in several forms. For many years, the generation of useful electric power from wind on the large scale has been centered predominantly on the use of rotating machinery, primarily wind turbines. While wind farms are known to be an effective means to generate power, their use is faced with several challenges, including prohibitive costs of infrastructure, including land, civil work, electrical work, transmission lines and approach roads. In addition, as the size of the turbine shrinks, concerns over efficiency, cost and reliability make room for novel designs for more efficient performance. In particular, small-scale devices that contain few mechanical parts have a greater potential owing to their reduced mechanical losses. One promising solution is to convert the fluid flow into a sort of mechanical vibration from which electric power can be extracted. The key aspect in this work, therefore, lies in converting fluid flow into some type of flow-induced vibration, which in turn can be converted into useful power.

Various alternative energy solutions based on wind harvesting have been proposed in the past few years. In an early study, Pike [4] proposed the use of the Magnus effect for a wind generator. Another endeavor has been reported by Jones *et al*. [5] who investigated power extraction from an

- *Mohammed Ali is with the Production Engineering and Printing Technology Department, Akhbar Elyom Academy, Egypt. (e-mail: eng.muhammedali@yahoo.com).*
- *Mustafa Arafa is with the Mechanical Engineering Department, American University in Cairo, Egypt (e-mail: mharafa@aucegypt.edu).*
- *Mohamed Elaraby is with the Department of Mechanical Design and Production, Faculty of Engineering, Cairo University, Egypt. (e-mail: prof_m_elaraby@yahoo.com).*

oscillating wing power generator based on the phenomenon of flutter. The concept of flutter was also developed by Frayne [6], who proposed an energy harvesting device that relies on a fluttering membrane fitted with a pair of magnets that oscillate between metal coils. More recently, Wang *et al*. [7] presented an electromagnetic energy harvester that exploits vortex shedding from bluff bodies placed in a flowing water stream. Reference is also made to the works of Jung and Lee [8] on utilizing wake galloping and Bibo *et al*. [9] who devised a micro wind power generator that mimics the oscillations of the reeds of music-playing harmonica.

This work addresses the concept of generating mechanical vibration from wind through the phenomenon of galloping, and exploiting the ensuing motion to harvest useful energy. The device being investigated for this purpose consists of a lightweight box that is mounted at the tip of a flexible cantilever beam facing an incoming wind stream. Wind-induced vibration causes the box to gallop in the transverse direction, leading to self-excited bending vibrations in the beam. Energy is harvested using electromagnetic energy transduction where a beam-mounted magnet moves past a stationary coil. While the concept has been recently investigated [10-13], emphasis in this work is placed on assessing the lift and drag coefficients numerically, and applying the resulting forces, together with their variation with the angle of attack, on a finite element model of the system in order to predict the dynamic behavior.

The remainder of this paper is organized into eight sections. Sections 2-4 present the design of the proposed energy harvester, together with the electromechanical modeling of the system, which comprises determination of the wind loads and formulation of a dynamic model to predict the output voltage as a function of the design parameters. Sections 5-7 present the experimental verification of the proposed design, and section 8 is dedicated to conclusions and recommendations.

2. DESIGN AND MODELING OF ENERGY HARVESTER

For many years, galloping has been known as an undesirable effect in transmission lines due to ice accretions in cold climates. Such ice formations can alter the original circular cross-section of the cables, leading to galloping oscillations in the vertical plane when the wind acts normal to the cable span. Pioneering contributions to the galloping problem are due to Den Hartog [14] who described an elementary apparatus for demonstrating galloping, which consists of a lightweight rod having a semicircular cross-section, suspended by springs in the vertical plane and subjected to cross wind. The susceptibility of structures to exhibit galloping depends on a number of variables including the variation of the lift and drag coefficients with the angle of attack. Various sections have been investigated in the literature, including rectangular [15], triangular [16], elliptical [17] and semicircular [11] sections. While galloping has been regarded as an undesirable effect in many structural applications, this phenomenon may well be exploited in energy harvesting applications.

Figure 1 shows a schematic illustration of the various designs being studied in this work. A lightweight solid cylindrical tip mass having a square, triangular, or semicircular cross-section is mounted at the tip of a flexible cantilever beam facing an incoming wind flow. Wind-induced vibration causes the box to gallop in the transverse direction, leading to self-excited bending vibrations in the beam. Energy is harvested due to the motion of the magnet past a stationary coil, whose terminals are connected across a load resistance.

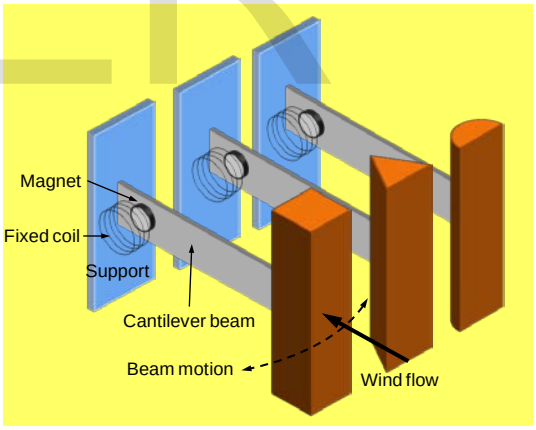

Fig. 1. Schematic illustration of proposed energy harvester.

3. ESTIMATION OF AIR LOADS

Figure 2 shows a square section undergoing both transverse and angular displacements denoted by w and θ, respectively. The structure is exposed to an air flow with a constant mean speed U.

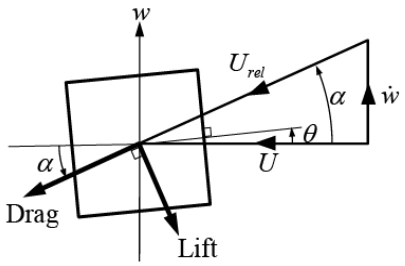

Fig. 2. Air loads acting on square section.

The generated lift (L) and drag (D) forces are given by [18] as:

$$L = \tfrac{1}{2}\rho U_{rel}^2 b\, C_L\big|_{\alpha-\theta} \quad (1)$$

and

$$D = \tfrac{1}{2}\rho U_{rel}^2 b\, C_D\big|_{\alpha-\theta} \quad (2)$$

where ρ is the air density, b is the product of the section width by the out-of-plane width, U_{rel} is the velocity of air relative to the section, and C_L and C_D are the lift and drag coefficients, respectively, evaluated at the effective angle of attack (α-θ) which depends on both the section rotation, θ, and transverse velocity, $\dot{w}$. From geometry, we note:

$$U_{rel}\cos\alpha = U \quad (3)$$

Resolving the lift and drag forces along the transverse direction gives:

$$F_A = -D\sin\alpha - L\cos\alpha \quad (4)$$

Which can be written as:

$$F_A = \tfrac{1}{2}\rho U^2 b \sec^2\alpha\left[-C_D\big|_{\alpha-\theta}\sin\alpha - C_L\big|_{\alpha-\theta}\cos\alpha\right] \quad (5)$$

or:

$$F_A = \tfrac{1}{2}\rho U^2 b C_A \quad (6)$$

where

$$C_A = \sec^2\alpha\left[-C_D\big|_{\alpha-\theta}\sin\alpha - C_L\big|_{\alpha-\theta}\cos\alpha\right] \quad (7)$$

and:

$$\alpha = \tan^{-1}\left(\frac{\dot{w}}{U}\right) \quad (8)$$

The lift and drag coefficients in Eqs. (1) and (2) are highly dependent on the section geometry, as well as the flow characteristics, mainly Reynolds number. Different studies have been reported in the literature to investigate the variation of the lift and drag coefficients with the angle of attack for rectangular sections. However, these studies are only available for limited angles of attack [19, 20] or lower Reynolds numbers than the ones addressed in this work [21, 22]. One way to alleviate these obstacles is to use polynomial estimates of the aerodynamic forces [23], but these are limited to Reynolds numbers below 200. To overcome this limitation, a finite element model will be established in this work to evaluate the lift and drag forces. The methodology will first be verified through comparisons with previous studies with similar flow conditions. The analysis will then be employed to model the present harvester.

A Computational Fluid Dynamic (CFD) model was first conducted to determine the resultant aerodynamic forces acting on a stationary bluff object subjected to an incoming wind stream. This model can be regarded as a "computational wind-tunnel test" on a square section to evaluate the lift and drag coefficients at various angles of attack. A two-dimensional model was developed on the multiphysics finite element analysis software COMSOL to solve the one-way fluid-structure interaction problem between a stationary rigid object (solid domain), tilted at various angles and placed within a flowing wind stream (fluid domain). The loads imparted by the fluid on the fixed object was determined by integrating the reaction forces on the mutual interaction surfaces along the direction parallel to the fluid flow (drag force) and the one perpendicular to it (lift force). The lift (C_L) and drag (C_D) coefficients are then obtained from:

$$C_L = \frac{2L}{\rho U^2 b} \quad , \quad C_D = \frac{2D}{\rho U^2 b} \quad (9)$$

A rectangular air domain, measuring 16.67 × 6.17 m, was discretized using free triangular mesh. A solid steel square section having a side of length 50 mm was inserted in the fluid flow at various angles of attack. Corners of the square section were rounded with a fillet radius of 0.7 mm to avoid mesh distortion. The width of the chosen wind tunnel was chosen sufficiently large compared to the obstacle size to avoid interactions with the tunnel walls. The number of elements in the model was systematically increased, reaching nearly 20,000 elements, until converged results were obtained. The wind velocity profile is assumed to be uniform, the turbulent intensity is taken as 5%, and the turbulence length scale is set to 0.014 m. The wind velocity of the stream at the inlet edge of the chamber is taken as 30 m/s, which yields a Reynolds number (based on the model characteristic length) of Re = 10^5 at zero angle of attack for the square section. This value enables

comparisons with the experimental work of Alonso *et al*. [22]. The top and bottom edges are modeled as fixed walls, whereas zero pressure was imposed at the outlet boundary.

The model is solved in two steps. First, a turbulent flow analysis is conducted to investigate the interaction between the test section and the fluid flow. This enables calculating the wall shear stresses due to viscous effects, and normal stresses due to fluid pressure. Subsequently, a solid mechanics model is implemented, wherein the output stresses produced from the previous step are applied on the solid domain to obtain the resultants of the reaction forces in the direction of the stream velocity and the direction normal to it. Figure 3 shows the velocity field distribution around the square section at 45° angle of attack.

A total of 19 runs were performed at angles of attack ranging from -45° to 45° to obtain the variation of the lift and drag coefficients.

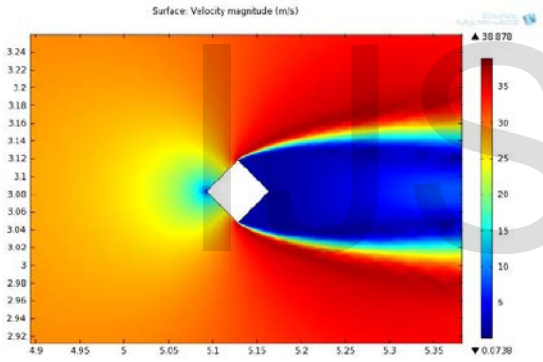

Fig. 3. Velocity profile around square section.

Figure 4 shows the results obtained by the present work in comparison with the experimental results of Alonso *et al*. [22]. The results show a close agreement for the lift coefficient. The general trend in the drag coefficient variation is also captured by the present formulation, but deviations reaching about 30% are noted for increasing angles of attack.

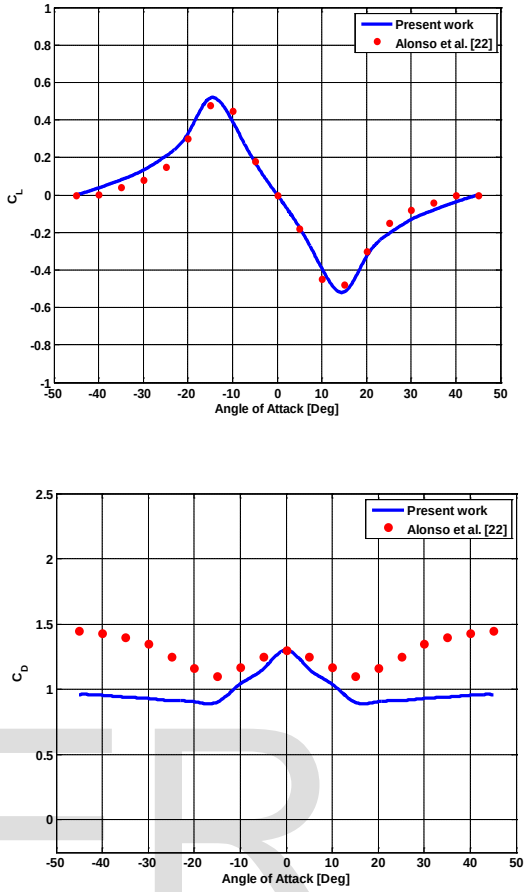

Fig. 4. Variation of lift and drag coefficient with the angle of attack.

As another comparison, the wind speed was reduced to 1 m/s, keeping all other parameters the same, in order to achieve a Reynolds number of Re = 3×10^3 thereby enabling comparison with the work of Mukhopadhyay [21]. The result is shown in Figure 5 which shows the variation of the aero-elastic lift coefficient, C_A, versus tan (α-θ). The results are shown to be in fair agreement, especially for smaller angles of attack. Discrepancies may be attributed to intricate details, such as the radius of the rounded corners which can significantly alter the drag characteristics.

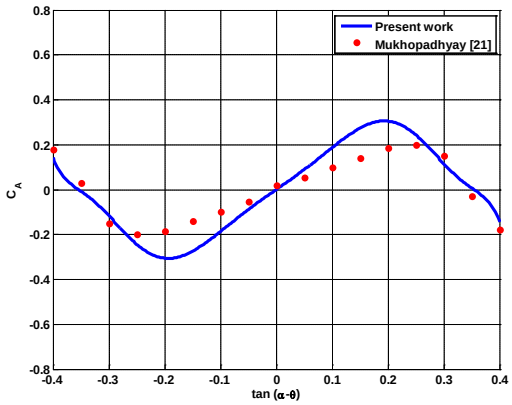

Fig. 5. Variation of aero-elastic force coefficient with the tan (α-θ) at Re = 3000

The same methodology described above was employed to obtain the lift and drag characteristics for an equilateral triangular and a semicircular section (D-section) under the same flow conditions. The wind speed was set to 3.25 m/s which provides Re = 10.8×10^3. Figures 6 and 7 show the velocity field around the triangular and D-section, respectively, at zero angle of attack.

A total of 73 runs were performed at angles of attack ranging from -180° to 180° to obtain the variation of the lift and drag coefficients for equilateral triangular section, and 37 runs were performed at angles of attack ranging from -90° to 90° to obtain the variation of the lift and drag coefficients for semicircular section.

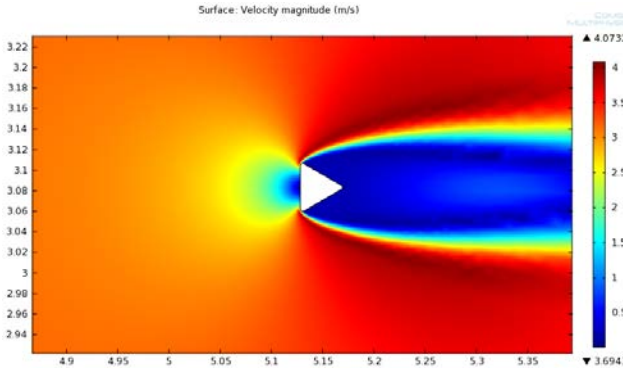

Fig. 6. Velocity profile around triangular section.

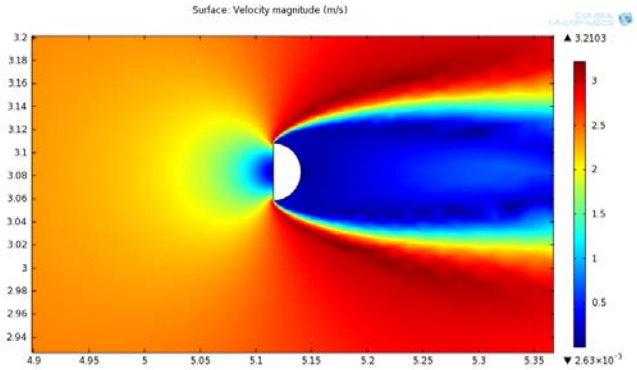

Fig. 7. Velocity profile around D- section.

Figures 8 and 9 show the results obtained by the present work in comparison with the experimental results of Alonso *et al*. [24] for equilateral triangular section, and with the experimental results of Ratkowski [25] for semicircular section.

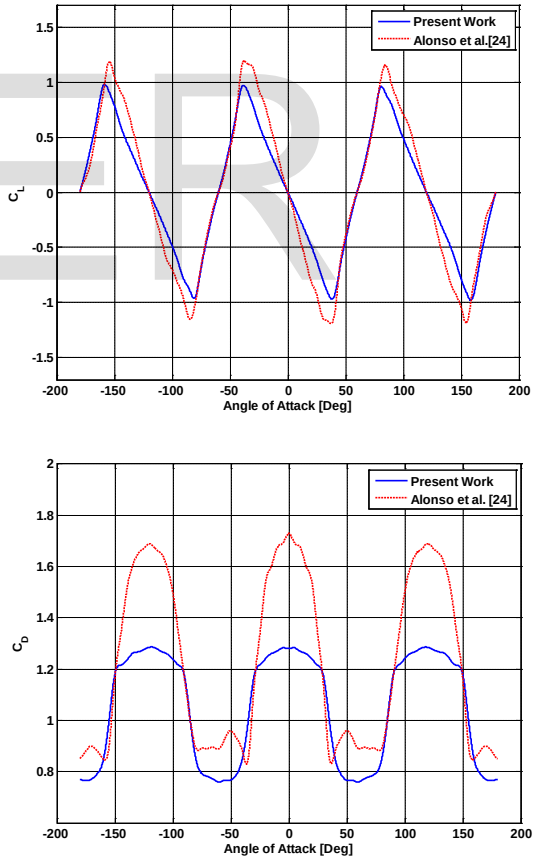

Fig.8. Variation of lift and drag coefficients with the angle of attack for a triangular cross section at Re = 10.8×10^3.

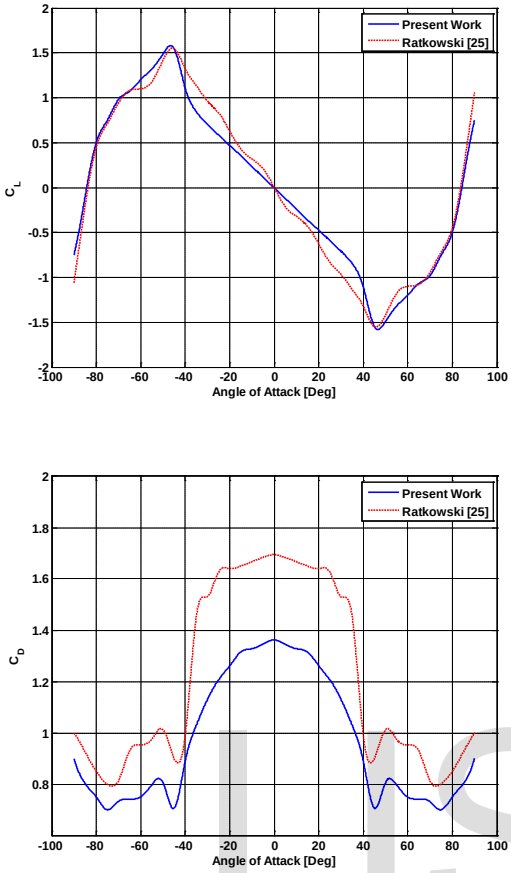

Fig. 9. Variation of lift and drag coefficients with the angle of attack for a D-section at Re = 10.8×10^3.

The results show the lift coefficient is in fair agreement. Discrepancies in the drag coefficient may be attributed to the radius of the rounded corners.

4. COUPLED ELECTO-AEROELASTIC MODEL

Using the Euler-Bernoulli beam formulation, a finite element model is formulated to study the dynamic behavior of the energy harvester. The beam was divided into 22 elements, each bounded by two nodes. Axial loading on the beam was neglected in this study. The vector of nodal degrees of freedom, $\{\delta\}$, is structured to contain the transverse displacements (odd numbered entries) and cross section rotations (even-numbered entries) in the displacement vector, i.e.

$$\{\delta\} = \{w_1 \quad \theta_1 \quad w_2 \quad \theta_2 \quad \cdots \quad w_{22} \quad \theta_{22}\}^T \qquad (10)$$

The coupled electro-aeroelastic problem is modeled by extending the formulation developed earlier by Poulin *et al.* [26], which accounts for the effect of inducing electromagnetic current in a single-degree-of-freedom system, to a system having a finite number of degrees of freedom by introducing a forcing term proportional to the induced current, which in turn is proportional to the magnet velocity, at its point of attachment. Rotational displacement of the magnet is neglected since it is placed close to the fixed end where the displacement is predominantly linear. The coupled equations governing the dynamic behavior of the system are expressed as:

$$\begin{bmatrix}[M] & \{0\} \\ \{0\} & 0\end{bmatrix}\begin{Bmatrix}\{\ddot{\delta}\} \\ \ddot{I}\end{Bmatrix}+\begin{bmatrix}[C] & \{0\} \\ \{P\} & -L_c\end{bmatrix}\begin{Bmatrix}\{\dot{\delta}\} \\ \dot{I}\end{Bmatrix}+\begin{bmatrix}[K] & \{P\}^T \\ \{0\} & -R_l-R_c\end{bmatrix}\begin{Bmatrix}\{\delta\} \\ I\end{Bmatrix}=\begin{Bmatrix}\{F\} \\ 0\end{Bmatrix} \qquad (11)$$

Where:

$$\{P\} = \{0 \quad 0 \quad 0 \quad 0 \quad BL_w \quad 0 \quad \cdots \quad 0\} \qquad (12)$$

In Eqs. (11) and (12), I is the current through the coil, B is the magnetic flux density (assumed to be constant), L_w is the total wire length, R_c is the coil resistance R_l is the load resistance, and L_c is the coil inductance. All entries of the vector $\{P\}$ in Eq. (12) are zeros except the fifth, which corresponds to the transverse structural displacement of the node on the beam where the magnet is attached.

The mass matrix is adjusted to include the mass of the magnet and its mass moment of inertia. The damping matrix in Eq. (11) is estimated as $[C] = \gamma [M] + \beta [K]$. This damping term only includes mechanical damping in the system whereas electromagnetic damping will be included in the force terms. The force vector $\{F\}$ in Eq. (11) accounts for both the aerodynamic forces (estimated in the previous section) applied at the beam tip and the electromagnetic damping force at the magnet location. Accordingly, entries in the force vector are listed as:

$$\{F\} = \{0 \quad 0 \quad 0 \quad 0 \quad F_n \quad 0 \quad \cdots \quad 0 \quad F_A \quad 0\}^T \qquad (13)$$

where F_A is the aerodynamic force and F_n is the electromagnetic force given by:

$$F_n = -BL_w I \qquad (14)$$

Equation (11) is numerically integrated in the time domain to obtain both the mechanical and electrical responses for a given input wind speed and load resistance. As an initial condition, the beam is perturbed from its equilibrium position to allow the oscillations to build up. In all simulations, all nodes were given zero initial displacements and slight initial velocities that are proportional to the beam's static deflection curve.

5. EXPERIMENTAL VALIDATION

Figure 10a shows a photograph of the experimental setup consisting of a stainless steel beam measuring 192 × 25.4 × 0.45 mm rigidly fixed to a bracket at one end. At the free end, one of the foam boxes shown in Figure 10b (each having a mass of 10 g) is firmly attached. The side facing the incoming wind stream measures 250 × 50 mm for all the boxes used in this study. A nickel plated cylindrical NdFeB button magnet having a diameter of 17 mm and a thickness of 2.3 mm is attached to the beam 26 mm away from the fixed end and a coil is fixed in front of it. Resistive load in the range from 100 Ω to 10 kΩ is provided by a decade resistance box (Lutron, type RBOX-408). Data is captured on a multi-channel dynamic signal analyzer (LMS Pimento).

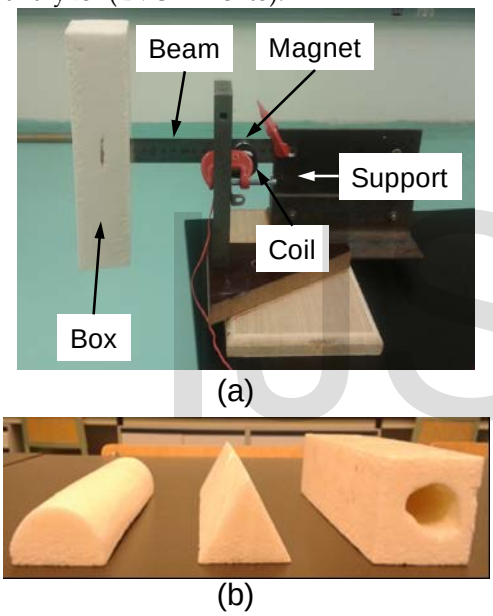

Fig. 10. (a) Experimental setup, (b) Tip end cross section.

This setup is subjected to a steady wind stream whose velocity was measured by a handheld metal vane anemometer. Once placed in the wind flow, the beam is allowed to oscillate from rest. The time-domain signal, including measurement of the amplitude build-up, is recorded for 30 seconds until steady-state oscillations are observed to prevail. Wind speeds of 3.25, 5.5, and 8.5 m/s were utilized in this work. The magnetic flux density was estimated for the average distance between the magnet and the coil based on data released by the magnet manufacturer [27]. Table 1 lists the geometrical and material properties relevant to this work.

TABLE 1: GEOMETRICAL AND MATERIAL PROPERTIES

Beam	
Modulus of Elasticity	207 GPa
Density	7800 kg/m^3
Thickness	0.45 mm
Width	25.4 mm
Beam Length	192 mm
Mechanical damping	
Assumed mass matrix coefficient (γ)	0 rad/s
Assumed stiffness matrix coefficient (β)	10^{-5} s/rad
Air Properties	
Air density (ρ)	1.184 kg/m^3
Electromagnetic system	
Magnetic flux density at average gap (B)	0.0155 Tesla
Coil thickness	14 mm
Coil outer diameter	18.25 mm
Coil inner diameter	9 mm
Coil wire diameter	0.11 mm
Coil wire resistivity	17×10^{-9} Ωm

6. TRANSIENT RESPONSE

As a sample, Figure 11 shows the time history plots of the output voltage, as predicted by the present model, for the square, triangular and D-sections for a load resistance of 5 kΩ and an air speed of 3.25 m/s. Figure 12 shows the corresponding experimentally measured voltages, which are shown to agree favorably with their theoretical counterparts.

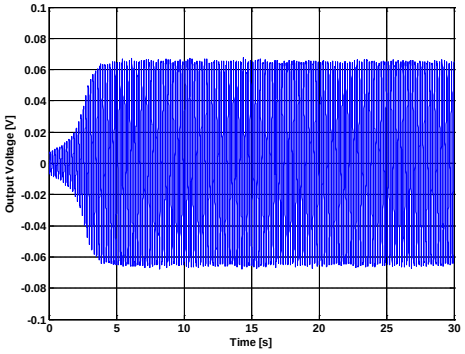

(a)

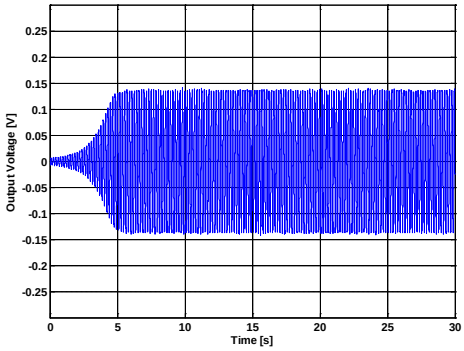

(b)

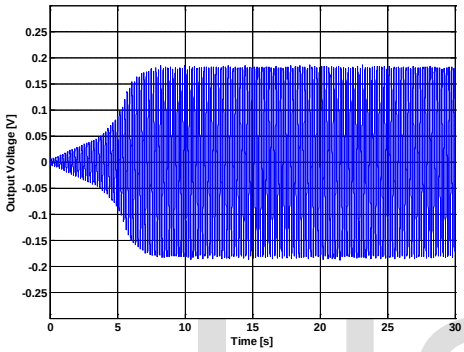

(c)

Fig. 11. Theoretical time history plots of output voltage (R_l = 5 kΩ, U=3.25 m/s) (a) Square section, (b) Triangular section, and (c) D- section.

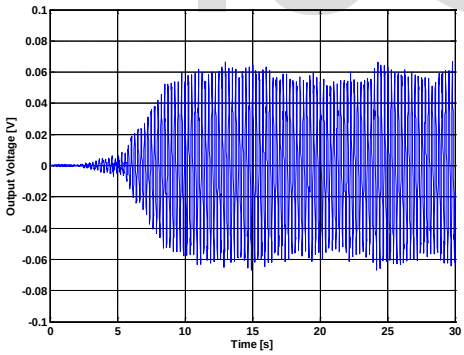

(a)

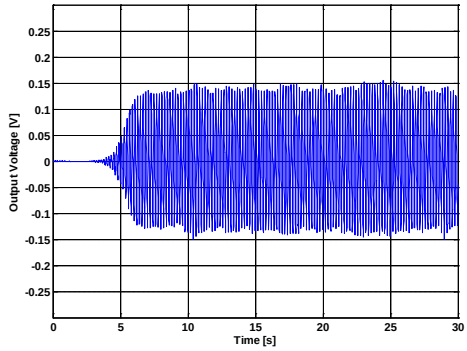

(b)

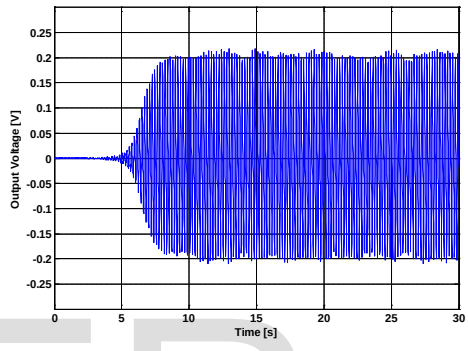

(c)

Fig. 12. Experimental time history plots of output voltage (R_l = 5 kΩ, U=3.25 m/s) (a) Square section, (b) Triangular section, and (c) D- section.

The experimental frequencies of vibration were found to be 3.65, 5.8 and 6.2 Hz for the square, triangular, and semicircular cross section, respectively, which agrees with the theoretical natural frequencies of 3.8, 6.1, and 6.5 Hz. These values were unaffected by wind speed or load resistance.

7. STEADY-STATE VOLTAGE AND POWER

Figures 13-18 show the theoretical and experimental output power and voltage as a function of load resistance for the different cross sections at wind speeds of 3.25, 5.5, and 8.5 m/s. The theoretical predictions are shown to compare favorably with experimental results. It is observed that maximum power is achieved at a load resistance of 300 Ω when using the semicircular box, which also agrees with the experimental results. For the magnet and coil used in this work, the maximum power achieved is approximately 100 μW.

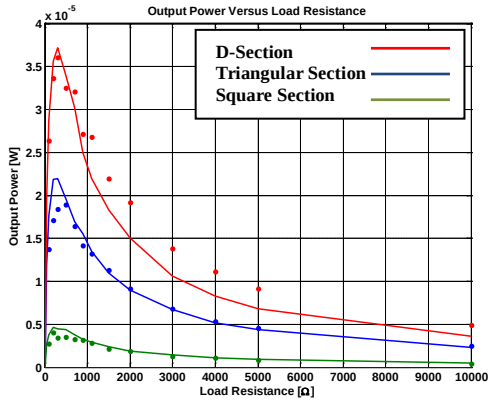

Fig. 13. Output power versus load resistance at wind speed of 3.25 m/s (• experimental measurements; — present model).

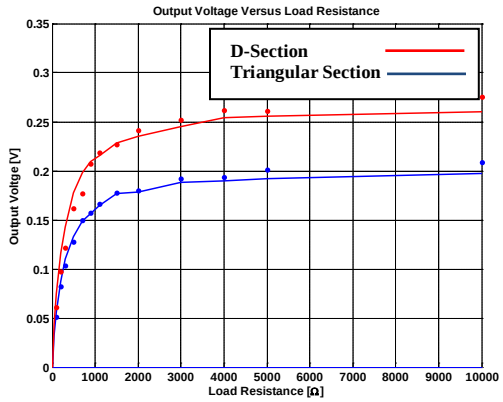

Fig. 16. Output voltage versus load resistance at wind speed of 5.5 m/s (• experimental measurements; — present model).

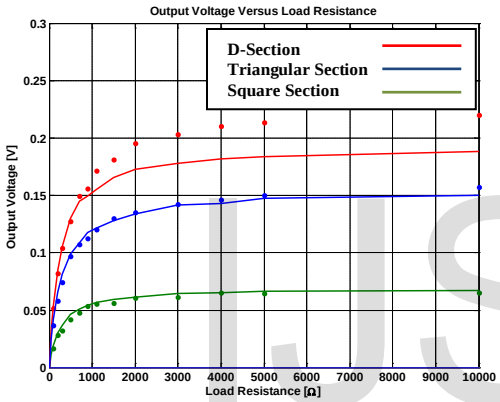

Fig. 14. Output voltage versus load resistance at wind speed of 3.25 m/s (• experimental measurements; — present model).

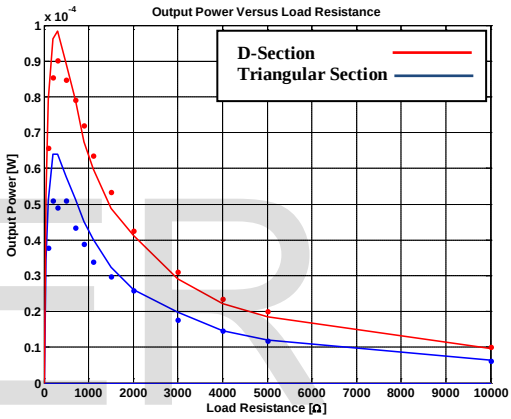

Fig. 17. Output power versus load resistance at wind speed of 8.5 m/s (• experimental measurements; — present model).

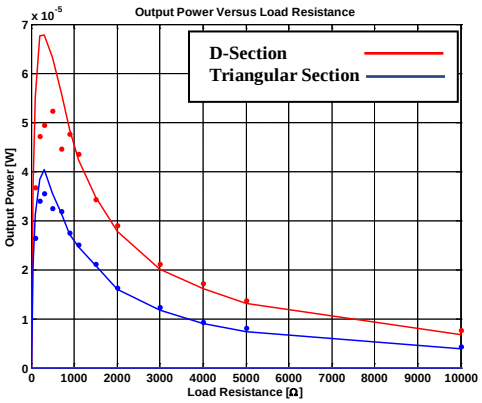

Fig. 15. Output power versus load resistance at wind speed of 5.5 m/s (• experimental measurements; — present model).

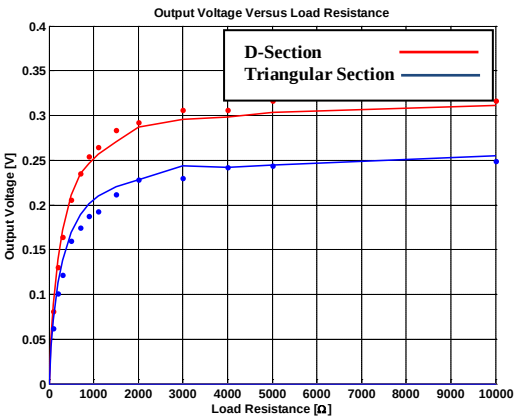

Fig. 18. Output voltage versus load resistance at wind speed of 8.5 m/s (• experimental measurements; — present model).

8. CONCLUSION

An electromagnetic energy harvester, based on the concept of galloping oscillations from an incoming steady wind stream, was developed in this work. A finite element model was formulated to evaluate the lift and drag coefficients of the galloping section. These characteristics were subsequently employed in a dynamic model to investigate the coupled electro-aeroelastic behavior of the proposed design. In general, the lift coefficients predicted in the present study were found to agree well with earlier experimental investigations reported in the literature, whereas the drag coefficients indicated some discrepancies in the magnitudes. However these variations were found not to influence the galloping behavior significantly. The theoretical model was supported by experimental validation at wind speeds of 3.25, 5.5, and 8.5 m/s for load resistances ranging from 100 Ω to 10 kΩ for three different cross sections of the tip mass. Of the geometries studied, the D-section was found to yield the greatest galloping behavior and hence the maximum power. The proposed design is envisaged to offer a viable solution for a standalone power source for remote wireless sensors.

ACKNOWLEDGMENT

The authors wish to thank Eng. Ahmed Abdel-Fattah for his useful input and contribution. The authors also acknowledge the support of Eng. Mostafa Gamal in conducting the finite element models.

REFERENCES

[1] A. Aladwani, M. Arafa, O. Aldraihem, and A. Baz, "Cantilevered Piezoelectric Energy Harvester with a Dynamic Magnifier," *ASME Journal of Vibration and Acoustics* 134 (3) (2012) 031004 (10 pages).

[2] M.M.R El-Hebeary, M.H. Arafa, and S.M. Megahed, "Modeling and Experimental Verification of Multi-modal Vibration Energy Harvesting from Plate Structures," *Sensors and Actuators A: Physical*, 193 (2013) 35-47.

[3] F. Najar, A.H. Nayfeh, E.M. Abdel-Rahman, S. Choura, and S. El-Borgi, "Dynamics and Global Stability of Beam-based Electrostatic Microactuators," *Journal of Vibration and Control* 16 (5) (2010) 721 - 748.

[4] D. Pike, "Rotor Power Ousts the Aerofoil," *New Scientist*, 30 August, 1984, 31-33.

[5] K.D. Jones, S. Davids, and M.F. Platzer, "Oscillating-wing Power Generation," *Proceedings of the 3rd ASME/JSME Joint Fluids Engineering Conference*, 1999, 1-6.

[6] S.M. Frayne, "Generator Utilizing Fluid-induced Oscillations," US Patent No. 7,573,143 B2, 2009.

[7] D.-A. Wang, C.-Y. Chiu and H.-T. Pham, "Electromagnetic Energy Harvesting from Vibrations Induced by Kármán Vortex Street," *Mechatronics* 22 (2012) 746-756.

[8] H.-J. Jung and S.-W. Lee, "The Experimental Validation of a New Energy Harvesting System based on the Wake Galloping Phenomenon," *Smart Materials and Structures*, vol. 20, no. 5, 2011.

[9] A. Bibo, G. Li and M. F. Daqaq, "Electromechanical Modeling and Normal Form Analysis of an Aeroelastic Micro-power Generator," *Journal of Intelligent Material Systems and Structures*, 22 (6) (2011) 577-592.

[10] J. Sirohi and R. Mahadik, "Piezoelectric Wind Energy Harvester for Low-power Sensors," *Journal of Intelligent Material Systems and Structures*, 22 (18) (2011) 2215-2228.

[11] A. Barrero-Gil, G. Alonso and A. Sanz-Andres, "Energy Harvesting from Transverse Galloping," *Journal of Sound and Vibration*, 329 (14) (2010) 2873–2883.

[12] A. Abdelkefi, M.R. Hajj, and A.H. Nayfeh, "Power Harvesting from Transverse Galloping of Square Cylinder," *Nonlinear Dynamics* 70 (2) (2012) 1355 – 1363.

[13] H.D. Akaydin, N. Elvin and Y. Andreopoulos, "The Performance of a Self-excited Fluidic Energy Harvester," *Smart Materials and Structures* 21 (2012) 025007 (13 pages)

[14] J.P. Den Hartog, *Mechanical Vibrations*, McGraw-Hill, 1956.

[15] N. Norberg, "Flow around Rectangular Cylinders: Pressure Forces and Wake Frequencies," *Journal of Wind Engineering and Industrial Aerodynamics* 49 (1993) 187 – 196.

[16] G. Alonso, J. Meseguer, and I. Pérez-Grande, "Galloping Stability of Triangular Cross-sectional Bodies: A Systematic Approach," *Journal of Wind Engineering and Industrial Aerodynamics* 95 (2007) 928 – 940.

[17] P. McComber, and A. Paradis, "A Aable Galloping Model for Thin ice Accretions," *Atmospheric Research* 46 (1998) 13 – 25.

[18] R. D. Blevins, *Flow-Induced Vibration*, 2nd Edition Edition, New York: Van Nostrand Reinhold, 1990.

[19] I. Robertson, L. Li, S. J. Sherwin and P. W. Bearman, "A Numerical Study of Rotational and Transverse Galloping Rectangular Bodies," *Journal of Fluids and Structures*, 17 (2003) 681–699.

[20] H. Lindner, "Simulation of the Turbulence Influence on Galloping Vibrations," *Journal of Wind Engineering and Industrial Aerodynamics*, 41-44 (1992) 2023-2034.

[21] V. Mukhopadhyay, *Wind excited vibration of square section beam and suspended cable*, DSc Thesis, Massachusetts Institute of Technology, 1972.

[22] G. Alonso, E. Valero, and J. Meseguer, "An Analysis on the Dependence on Cross Section Geometry of Galloping Stability of Two-dimensional Bodies having either Biconvex or Rhomboidal Cross Sections," *European Journal of Mechanics* 28 (2009) 328–334.

[23] A. Barrero-Gil, A. Sanz-Andres, and M. Roura, "Transverse Galloping at Low Reynolds Number," *Journal of Fluids and Structures* 25 (2009) 1236–1242.
[24] G. Alonso, J. Meseguer, "A Parametric Study of the Galloping Stability of Two-dimensional Triangular Cross-section Bodies," *Journal of Wind Engineering and Industrial Aerodynamics* 94 (2006) 241–253.
[25] J.J. Ratkowski, "Experimental with Galloping Spans," *AIEE Winter General Meeting 62* (1963) 661–669.
[26] G. Poulin, E. Sarraute and F. Costa, "Generation of Electrical Energy for Portable Devices: Comparative Study of an Electromagnetic and a Piezoelectric System," *Sensors and Actuators,* 116 (3) (2004) 461-471.
[27] http://www.kjmagnetics.com [accessed 30 November 2012].